

# GN-Net: The Gauss-Newton Loss for Multi-Weather Relocalization

Lukas von Stumberg<sup>1,2\*</sup> Patrick Wenzel<sup>1,2\*</sup> Qadeer Khan<sup>1,2</sup> Daniel Cremers<sup>1,2</sup>

**Abstract**—Direct SLAM methods have shown exceptional performance on odometry tasks. However, they are susceptible to dynamic lighting and weather changes while also suffering from a bad initialization on large baselines. To overcome this, we propose GN-Net: a network optimized with the novel Gauss-Newton loss for training weather invariant deep features, tailored for direct image alignment. Our network can be trained with pixel correspondences between images even from different sequences. Experiments on both simulated and real-world datasets demonstrate that our approach is more robust against bad initialization, variations in day-time, and weather changes thereby outperforming state-of-the-art direct and indirect methods. Furthermore, we release an evaluation benchmark for relocalization tracking against different types of weather. Our benchmark is available at <https://vision.in.tum.de/gn-net>.

## I. INTRODUCTION

In recent years, very powerful SLAM algorithms have been proposed [1], [2]. In particular, direct visual SLAM methods have shown great performance, outperforming indirect methods on most benchmarks [3], [4], [5]. They directly leverage the brightness data of the sensor in order to estimate localization and 3D maps rather than extracting a heuristically selected sparse subset of feature points. As a result, they exhibit a boost in precision and robustness. Nevertheless, compared to indirect methods, direct methods suffer from two major drawbacks:

- 1) Direct methods need a good initialization, making them less robust for large baseline tracking or cameras with a low frame rate.
- 2) Direct methods cannot handle changing lighting/weather conditions. In such situations, their advantage of being able to pick up very subtle brightness variations actually becomes a disadvantage to the more lighting invariant features.

Previously, deep learning-based approaches which try to overcome the problem of multiple-daytime tracking have converted nighttime images to daytime images, *e.g.* using GANs [6], [7], [8]. But the question arises why should images be the best input data representation for SLAM algorithms? Could there be better alternate representations?

This paper addresses the problem of adapting direct SLAM methods to challenging lighting and weather conditions. In this work, we show how to convert images into a multi-dimensional feature map which is invariant to lighting/weather changes and has a larger convergence basin. Thereby we overcome the aforementioned problems

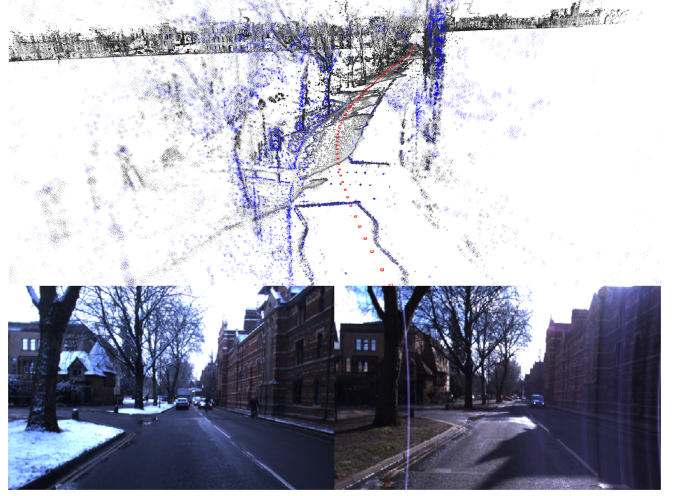


Fig. 1: We relocalize a snowy sequence from the Oxford RobotCar Dataset in a pre-built map created using a sunny weather condition. The points from the prior map (gray) are overlaid with the new points from the current run (blue), showing that the relocalization is accurate.

simultaneously. The deep features are trained with a novel Gauss-Newton loss formulation in a self-supervised manner. We employ a Siamese network trained with labels obtained either from simulation data or any state-of-the-art SLAM algorithm. This eliminates the additional cost of human labeling required for training the network. We leverage the fact that the linear system built in the Gauss-Newton algorithm used in direct image alignment also represents a probability distribution for each pixel. Starting from an initial solution, the Gauss-Newton loss is designed to maximize the probability of the correct correspondence. This results in features with a larger convergence basin compared to grayscale images. The superiority of our method stems from its ability to generate these multi-channel, weather-invariant deep features that facilitate relocalization across different weathers. Figure 1 shows how our method can successfully relocalize a snowy sequence in a pre-built map created using a sunny sequence.

In common benchmarks [9], localizing accurately in a pre-built map has been tackled by finding nearby images and tracking the relative pose (6DOF) between them. However, we propose to split this into two separate tasks and focus only on the latter. This way, we can evaluate its performance in isolation. This is formalized to what we refer to as *relocalization tracking*. Since there is no publicly available dataset to evaluate *relocalization tracking* performance across multiple

\*These authors contributed equally.

<sup>1</sup>Technical University of Munich

<sup>2</sup>Artisense

types of weathers, we are releasing an evaluation benchmark having the following 3 attributes:

- It contains sequences from multiple different weathers.
- Pixel-wise correspondences between sequences are provided for both simulated and real-world datasets.
- It decouples relocalization tracking from the image retrieval task.

The challenge here in comparison with normal pose estimation datasets [10], [11] is that the images involved are usually captured at different day-times/seasons and there is no good initialization of the pose.

We summarize the main contributions of our paper as follows:

- We derive the Gauss-Newton loss formulation based on the properties of direct image alignment and demonstrate that it improves the robustness to large baselines and illumination/weather changes.
- Our experimental evaluation shows, that GN-Net outperforms both state-of-the-art direct and indirect SLAM methods on the task of *relocalization tracking*.
- We release a new evaluation benchmark for the task of *relocalization tracking* with ground-truth poses. It is collected under dynamic conditions such as illumination changes, and different weathers. Sequences are taken from the the CARLA [12] simulator as well as from the Oxford RobotCar Dataset [13].

## II. RELATED WORK

We review the following main areas of related work: visual SLAM, visual descriptor learning, deep direct image alignment, and image-based relocalization in SLAM.

**Direct versus indirect SLAM methods:** Most existing SLAM systems that have used feature descriptors are based on traditional manual feature engineering, such as ORB-SLAM [2], MonoSLAM [14], and PTAM [1].

An alternative to feature-based methods is to skip the pre-processing step of the raw sensor measurements and rather use the pixel intensities directly. Popular direct methods are for RGB-D: DVO [15], and Kinect Fusion [16], and for cameras: DTAM [17], LSD-SLAM [3], DSO [4], and PhotoBundle [5]. However, the main limitation of direct methods is the *brightness constancy* assumption which is rarely fulfilled in any real-world robotic application [18]. The authors of [19] propose to use binary feature descriptors for direct tracking called Bit-planes. While improving the robustness to bad lighting situations it was also found that Bit-planes have a smaller convergence basin than intensities. This makes their method less robust to bad initialization. In contrast, the features we propose *both* improve robustness to lighting and the convergence basin.

**Visual descriptor learning:** Feature descriptors play an important role in a variety of computer vision tasks. For example, [20] proposed a novel correspondence contrastive loss which allows for faster training and demonstrates their effectiveness for both geometric and semantic matching across intra-class shape or appearance variations. In [21],

a deep neural network is trained using a contrastive loss to produce viewpoint- and lighting-invariant descriptors for the application of single-frame localization. [22] shows how to use convolutional neural networks to compute descriptors which allow for efficient detection of poorly textured objects and estimation of their 3D pose. In [23], the authors propose to train features for optical flow estimation using a Hinge loss based on correspondences. In contrast to our work, their loss function does not have a probabilistic derivation and they do not apply their features to pose estimation. [24] uses deep learning to improve SLAM performance in challenging situations. They synthetically create images and choose the one with most gradient information as the ground-truth for training. In contrast to them, we do not limit our network to output images similar to the real world. In [25], the authors compare dense descriptors from a standard CNN, SIFT, and normal image intensities for dense Lucas-Kanade tracking. There, it can be seen that grayscale values have a better convergence basin than the other features, which is something we overcome with our approach. In contrast to our work, they do not train the CNN architecture for their specific use case and they also apply it to optical flow instead of SLAM.

**Deep direct image alignment:** BA-NET [26] introduces a network architecture to solve the structure from motion (SfM) problem via feature-metric bundle adjustment. Unlike the BA-NET, instead of predicting the depth and the camera motion simultaneously, we propose to only train on correspondences obtained from a direct SLAM system. The advantage is that correspondences are oftentimes easier to obtain than accurate ground-truth poses. Furthermore, we combine our method with a state-of-the-art direct SLAM system and utilize its depth estimation, whereas BA-NET purely relies on deep learning. RegNet [27] is another line of work which tries to replace the handcrafted numerical Jacobian by a learned Jacobian with the help of a depth prediction neural network. However, predicting a dense depth map is often inaccurate and computationally demanding. The authors of [28] propose to use a learning-based inverse compositional algorithm for dense image alignment. The drawback of this approach is that the algorithm is very sensitive to the data distribution and constrained towards selecting the right hyperparameters.

**Relocalization:** An important task of relocalization is to approximate the pose of an image by simply querying the most similar image from a database [29], [30]. However, this has only limited accuracy since the 6DOF pose between the queried and the current image is not estimated. This can be done in a second step by 3D structure-based localization. Typically, this works by matching 2D-3D correspondences between an image and a point cloud and estimating the pose using indirect image alignment [31]. In contrast, we propose to use direct image alignment paired with deep features for this step.

**Relocalization benchmarks:** The authors of [9] have done sequence alignment on the Oxford RobotCar dataset, however, they have not made the matching correspondences

public. The Phototourism [32] is another dataset providing images and ground-truth correspondences of popular monuments from different camera angles and across different weather/lighting conditions. However, since the images are not recorded as a sequence, relocalization tracking is not possible. Furthermore, their benchmark only supports submission of features rather than poses, thereby restricting evaluation to only indirect methods.

### III. LOSS FUNCTIONS FOR DEEP DIRECT SLAM

In this work, we argue that a network trained to output features which produce better inputs for direct SLAM as opposed to normal images should have the following properties:

- Pixels corresponding to the same 3D point should have similar features.
- Pixels corresponding to different 3D points should have dissimilar features.
- When starting in a vicinity around the correct pixel, the Gauss-Newton algorithm should move towards the correct solution.

For optimizing the last property, we propose the novel Gauss-Newton loss which makes use of the probabilistic background of the Gauss-Newton algorithm for direct image alignment. The final loss used is a weighted sum of the pixel-wise contrastive loss and the Gauss-Newton loss.

**Architecture:** We are interested in learning a non-linear mapping  $f(x)$ , which maps images,  $\mathbb{R}^{W \times H \times C}$  to a dense visual descriptor space,  $\mathbb{R}^{W \times H \times D}$ , where each pixel is represented by a  $D$ -dimensional vector. The training is performed by a Siamese network architecture as shown in Figure 2, where we feed a pair of images,  $I_a$  and  $I_b$ , producing multi-scale feature pyramids  $F_a^l$  and  $F_b^l$ , where  $l$  represents the level of the decoder. For each image pair, we use a certain number of matches, denoted by  $N_{\text{pos}}$ , and a certain number of non-matches, denoted by  $N_{\text{neg}}$ . A pixel  $u_a \in \mathbb{R}^2$  from image  $I_a$  is considered to be a positive example if the pixel  $u_b \in \mathbb{R}^2$  from image  $I_b$  corresponds to the same 3D vertex (Figure 3). We make use of the inherent multi-scale hierarchy of the U-Net [33] architecture to apply the different loss terms from coarser to finer scaled pyramid levels. With this approach, our learned features will have a larger convergence radius for visual SLAM methods. More details on the network architecture are provided in the supplementary material.

**Pixelwise contrastive loss:** The pixelwise contrastive loss attempts to minimize the distance between positive pairs, and maximize the distance between negative pairs. It can be computed as follows:  $\mathcal{L}_{\text{contrastive}}(F_a, F_b, l) = \mathcal{L}_{\text{pos}}(F_a, F_b, l) + \mathcal{L}_{\text{neg}}(F_a, F_b, l)$ .

$$\mathcal{L}_{\text{pos}}(F_a, F_b, l) = \frac{1}{N_{\text{pos}}} \sum_{N_{\text{pos}}} D_{\text{feat}}^2 \quad (1)$$

$$\mathcal{L}_{\text{neg}}(F_a, F_b, l) = \frac{1}{N_{\text{neg}}} \sum_{N_{\text{neg}}} \max(0, M - D_{\text{feat}})^2 \quad (2)$$

where  $D_{\text{feat}}(\cdot)$  is the  $L_2$  distance between the feature embeddings:  $D_{\text{feat}} = \|F_a^l(u_a) - F_b^l(u_b)\|_2$  and  $M$  is the margin and set to 1.

**Gauss-Newton algorithm for direct image alignment:** We start with a review of direct image alignment (based on the frame-to-frame tracking from DSO). The input to this algorithm is a reference image with known depths for some pixels in the image, and a target image. The output is the predicted relative pose  $\xi$  between the two images. Starting from an initial guess the following algorithm is performed iteratively:

- 1) All pixels  $\mathbf{p}$  with known depth values are projected from the reference image  $\mathbf{I}$  into the target image  $\mathbf{I}'$  yielding the point  $\mathbf{p}'$ . For each of them a residual is computed, saying that the reference pixel and the target pixel should be similar:

$$r_i(\mathbf{p}, \mathbf{p}') = \mathbf{I}'(\mathbf{p}') - \mathbf{I}(\mathbf{p}) \quad (3)$$

- 2) For each residual the derivative with respect to the relative pose is:

$$\mathbf{J}_i = \frac{dr_i}{d\xi} = \frac{d\mathbf{I}'(\mathbf{p}')}{d\mathbf{p}'} \cdot \frac{d\mathbf{p}'}{d\xi} \quad (4)$$

Notice that the reference point  $\mathbf{p}$  does not change for different solutions  $\xi$ , therefore it does not appear in the derivative.

- 3) Using the stacked residual vector  $\mathbf{r}$ , the stacked Jacobian  $\mathbf{J}$  and a diagonal weight matrix  $\mathbf{W}$ , the Gaussian system and the step  $\delta$  is computed as follows:

$$\mathbf{H} = \mathbf{J}^T \mathbf{W} \mathbf{J} \text{ and } \mathbf{b} = -\mathbf{J}^T \mathbf{W} \mathbf{r} \text{ and } \delta = \mathbf{H}^{-1} \mathbf{b} \quad (5)$$

In the computation of the Jacobian the numerical derivative of the image  $\frac{d\mathbf{I}'(\mathbf{p}')}{d\mathbf{p}'}$  is used. As typical images are extremely non-convex this derivative is only valid in a small vicinity (usually 1-2 pixels) around the current solution which is the main reason why direct image alignment needs a very good initialization. To partially overcome this, a pyramid scheme is often used to increase the convergence radius.

We propose to replace the image  $\mathbf{I}$  with a feature map computed by a deep neural network. We still run the same algorithm as it would be done for a multi-channel (e.g. color) image. The only difference to the above formulas is that now we have multiple residuals for each pixel (one for each channel of the feature map). Usually tracking on multiple channels instead of one can decrease the convergence radius ([19], [25]). However, in our case, we train the feature maps to in fact have a larger convergence radius.

**Gauss-Newton on individual pixels:** Instead of running the Gauss-Newton algorithm on the full pose we can instead also run it on individual pixels (which is similar to the Lucas-Kanade algorithm [34]). This simplifies the Jacobian:

$$\mathbf{J} = \frac{d\mathbf{I}'(\mathbf{p}')}{d\mathbf{p}'} \quad (6)$$

In this case, the Hessian will be a 2-by-2 matrix and our step  $\delta$  can simply be added to the current pixel position.

Note that our simplified Jacobian differs from the one for full pose estimation (Equation (4)) only by the derivative

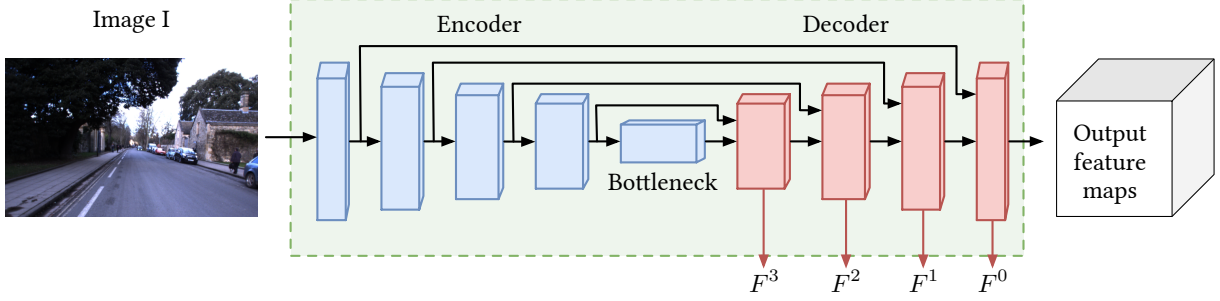


Fig. 2: Overview of one branch of the Siamese network architecture. Each branch is a modified U-Net [33] architecture which receives as an input an image and predicts multi-scale feature maps  $[F^0, F^1, F^2, F^3]$ . The multi-scale feature maps from the decoder network of both branches are then passed and used by DSO. Note that the weights between the two branches are shared.

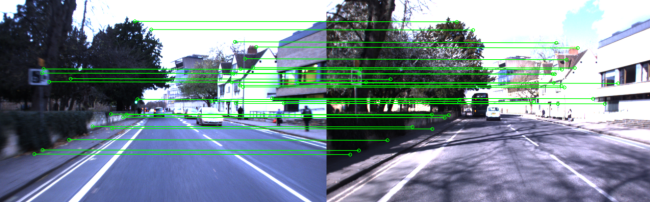


Fig. 3: This figure shows training correspondences between a pair of images from our benchmark.

with respect to the pose  $\frac{d\mathbf{p}'}{d\xi}$  which is much smoother than the image derivative. This means that if the Gauss-Newton algorithm performs well on individual pixels it will also work well on estimating the full pose. Therefore, we propose to train a neural network on correspondences which are easy to obtain, *e.g.* using a SLAM method, and then later apply it for pose estimation.

How do we determine if a feature map performs well on this task? Intuitively, the Gauss-Newton step should move the correspondence into the right direction if initialized in the vicinity of the correct solution. We would also like the network to be able to represent the certainty of its solution which is why we propose to use the Gauss-Newton loss.

**The probabilistic Gauss-Newton loss:** From now on, we will focus on the 2-dimensional Gaussian distribution, as we want to optimize the 2D pixel location on an image. The idea behind the Gauss-Newton algorithm is to maximize the probability of the solution.

To find the mean  $\mu$  which also represents the solution with maximum probability, we minimize the negative log-likelihood:

$$E(\mathbf{x}) = -\log f_X(\mathbf{x}) = \quad (7)$$

$$\frac{1}{2}(\mathbf{x} - \mu)^T \Sigma^{-1}(\mathbf{x} - \mu) + \log(2\pi\sqrt{|\Sigma|}) = \quad (8)$$

$$\frac{1}{2}(\mathbf{x} - \mu)^T \mathbf{H}(\mathbf{x} - \mu) + \log(2\pi) - \frac{1}{2} \log(|\mathbf{H}|) \quad (9)$$

In the Gauss-Newton algorithm the mean is computed with  $\mu = \mathbf{x} + \delta$ , where the  $\delta$  comes from Equation (5). To derive this, only the first term is used (because the latter parts are constant for all solutions  $\mathbf{x}$ ). In our case, however, the second

term is very relevant, because the network has the ability to influence both  $\mu$  and  $\mathbf{H}$ .

This derivation shows, that  $\mathbf{H}$ ,  $\mathbf{b}$  as computed in the GN-algorithm, also define a Gaussian probability distribution with mean  $\mathbf{x} + \mathbf{H}^{-1}\mathbf{b}$  and covariance  $\mathbf{H}^{-1}$ .

When starting with an initial solution the goal of our network should be to maximize the estimated probability of the correct pixel. With  $\mathbf{x}$  being the correct correspondence, we therefore use  $E(\mathbf{x}) = \text{Equation (9)}$  as our loss function which we call the *Gauss-Newton Loss* (see Algorithm 1).

---

**Algorithm 1** Compute Gauss-Newton Loss

---

```

 $f_1 \leftarrow \text{network}(I_a)$ 
 $f_2 \leftarrow \text{network}(I_b)$ 
 $e \leftarrow 0$  ▷ Total error
for all correspondences  $x_1, x_2$  do
   $f_t \leftarrow f_1(x_1)$  ▷ Target feature
   $x_s \leftarrow x_2 + \text{rand}(\text{vicinity})$  ▷ Compute start point
   $f_s \leftarrow f_2(x_s)$ 
   $r \leftarrow f_s - f_t$  ▷ Residual
   $J \leftarrow \frac{df_2}{dx_s}$  ▷ Numerical derivative
   $H \leftarrow J^T J + \epsilon \cdot \text{Id}$  ▷ Added epsilon for invertibility
   $b \leftarrow J^T r$ 
   $\mu \leftarrow x_s - H^{-1}b$ 
   $e_1 \leftarrow \frac{1}{2}(x_2 - \mu)^T H(x_2 - \mu)$  ▷ First error term
   $e_2 \leftarrow \log(2\pi) - \frac{1}{2} \log(|H|)$  ▷ Second error term
   $e \leftarrow e + e_1 + \lambda e_2$ 
end for

```

---

In the algorithm, a small number  $\epsilon$  is added to the diagonal of the Hessian, to ensure it is invertible. Also, the second energy term is weighted by  $\lambda$ .

**Analysis of the Gauss-Newton loss:** By minimizing Equation (9) the network has to maximize the probability density of the correct solution. As the integral over the probability densities always has to be 1, the network has the choice to either focus all the density on a small set of solutions (with more risk of being penalized if this solution is wrong), or to distribute the density to more solutions which in turn will have a lower individual density. By maximizing the probability of the correct solution, the network is incentivized to improve the estimated solution and its certainty.

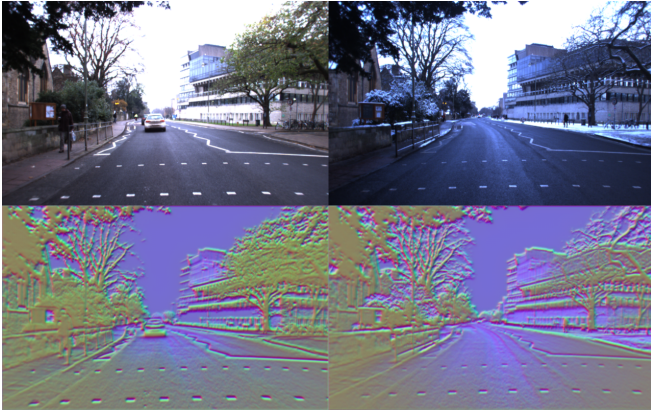


Fig. 4: This figure shows images and their corresponding feature maps predicted by our GN-Net for the Oxford RobotCar dataset. Each column depicts the image and feature map for a sample taken from 2 different sequences. Despite lighting and weather changes, the feature maps are robust to these variations. The visualization of the features shows the high-dimensional descriptors reduced to 3D through PCA.

This is also reflected in the two parts of the loss. The first term  $e_1 = \frac{1}{2}(\mathbf{x} - \boldsymbol{\mu})^T \mathbf{H}(\mathbf{x} - \boldsymbol{\mu})$  penalizes deviations between the estimated and the correct solution, scaled with the Hessian  $\mathbf{H}$ . The second term  $e_2 = \log(2\pi) - \frac{1}{2} \log(|\mathbf{H}|)$  is large if the network does not output enough certainty for its solution. This means that the network can reduce the first error term  $e_1$  by making  $\mathbf{H}$  smaller. As a consequence, the second error term will be increased, as this will also reduce the determinant of  $\mathbf{H}$ .

Notice also that this can be done in both dimensions independently. The network has the ability to output a large uncertainty in one direction, but a small uncertainty in the other direction. This is one of the traditional advantages of direct methods which are naturally able to utilize also lines instead of just feature points.

From Equation (9) it can be observed that the predicted uncertainty depends only on the numerical derivative of the target image at the start position. The higher the gradients the higher the predicted certainty. In DSO this is an unwanted effect which is counteracted by the gradient-dependent weighting applied to the cost-function [4, Equation (7)]. In our case, however, it gives the network the possibility to express its certainty and incentivizes it to output discriminative features.

Upon training the network with our loss formulation, we observe that the features are very similar despite being generated from images taken from sequences with different lighting/weather conditions, as shown in Figure 4.

#### IV. RELOCALIZATION TRACKING BENCHMARK

Previous tasks for localization/odometry can primarily be divided into two categories:

- Odometry datasets [10], [11], where there is a continuous stream of images (sometimes combined with additional sensor data like IMUs).

- Image collections where individual images are usually further apart from each other in space and time [35], [9].

We argue that for a number of applications a combination of these two tasks which we refer to as *relocalization tracking* is a more realistic scenario. The idea is that the algorithm has two inputs:

- 1) An image sequence (like a normal odometry dataset).
- 2) A collection of individual images (possibly with different weathers/times), each of which shall be tracked against one specific image from point 1.

The algorithm is supposed to track the normal sequential image sequence and at the same time perform tracking of the images in point 2. The advantage of this task is that the used algorithm can utilize the temporally continuous sequence from point 1 to compute accurate depth values for a part of the image (using a standard visual odometry method), which can then be used to improve the tracking of the individual images of point 2.

This task is very realistic as it comes up when tracking an image sequence and at the same time trying to relocalize this sequence in a prior map. A similar challenge occurs by trying to merge multiple maps from different times. In both cases, one has more information than just a random collection of images. It is important to reiterate here that the task of finding relocalization candidates is not considered but rather trying to track them with maximum accuracy/robustness is the focus. This is because our benchmark decouples image retrieval from tracking.

We have created a benchmark for *relocalization tracking* using the CARLA simulator and the Oxford RobotCar Dataset. Our benchmark includes ground-truth poses between different sequences for both training, validation, and testing.

**CARLA:** For synthetic evaluations, we use CARLA version 0.8.2. We collect data for 3 different weather conditions representing *WetNoon*, *SoftRainNoon*, and *WetCloudySunset*. We recorded the images at a fixed framerate of 10 frames per second (FPS). At each time step, we record images and its corresponding dense depth map from 6 different cameras with different poses rendered from the simulation engine, which means that the poses in the benchmark are not limited to just 2 DOF. The images and the dense depth maps are of size  $512 \times 512$ . For each weather condition, we collected 3 different sequences comprising 500-time steps. This is done for training, validation, and testing, meaning there are 27 sequences, containing 6 cameras each. Training, validation and test sequences were all recorded in different parts of the CARLA town. We have generated the test sequences after all hyperparameter tuning of our method was finished, meaning we ourselves had no access to the test data when developing the method. In accordance, we shall withhold the ground-truth for the test sequences of the benchmark.

**Oxford RobotCar:** Creating a multi-weather benchmark for this dataset imposes various challenges because the GPS-based ground-truth is very inaccurate. To find the relative poses between images from different sequences we have

used the following approach. For pairs of images from two different sequences, we accumulate the point cloud captured by the 2D lidar for 60 meters using the visual odometry result provided by the Oxford dataset. The resulting two point clouds are aligned with the global registration followed by ICP alignment using the implementation of Open3D [36]. We provide the first pair of images manually and the following pairs are found using the previous solution. We have performed this alignment for the following sequences: *2014-12-02-15-30-08 (overcast)* and *2015-03-24-13-47-33 (sunny)* for training. For testing, we use the reference sequence *2015-02-24-12-32-19 (sunny)* and align it with the sequences *2015-03-17-11-08-44 (overcast)*, *2014-12-05-11-09-10 (rainy)*, and *2015-02-03-08-45-10 (snow)*.

## V. EXPERIMENTAL EVALUATION

We perform our experiments on the *relocalization tracking* benchmark described in Section IV. We demonstrate the multi-weather relocalization performance on both the CARLA and the Oxford RobotCar dataset. For the latter, we show that our method even generalizes well to unseen weather conditions like rain or snow while being trained only on the sunny and overcast conditions.

Furthermore, a qualitative relocalization demo<sup>1</sup> on the Oxford RobotCar dataset is provided, where we demonstrate that our GN-Net can facilitate precise relocalization between weather conditions.

We train our method using sparse depths created by running Stereo DSO on the training sequences. We use intra-sequence correspondences calculated using the DSO depths and the DSO pose. Meanwhile, inter-sequence correspondences are obtained using DSO depths and the ground-truth poses provided by our benchmark. The ground truth poses are obtained via Lidar alignment for Oxford and directly from the simulation engine for CARLA as explained in section IV. Training is done from scratch with randomly initialized weights and an ADAM optimizer with a learning rate of  $10^{-6}$ . The image pair fed to the Siamese network is randomly selected from any of the training sequences while ensuring that the images in the pair do not differ by more than 5 keyframes. Each branch of the Siamese network is a modified U-Net architecture with shared weights. Further details of the architecture and training can be found in the supplementary material. Note that at inference time, only one image is needed to extract the deep visual descriptors, used as input to the SLAM algorithm. While in principle, our approach can be deployed in conjunction with any direct method, we have coupled our deep features with Direct Sparse Odometry (DSO).

The following methods are evaluated:

**Direct Sparse Odometry (DSO):** The stereo odometry method [37] based on [4] is used. Whenever there is a relocalization candidate for a frame we ensure that the system creates the corresponding keyframe. This candidate is tracked using the *coarse tracker*, which performs direct

image alignment in a pyramid scheme. We use the identity as initialization without any other random guesses for the pose.

**GN-Net (Ours):** Same as with DSO, however, for relocalization tracking, we replace the grayscale images with features created by our GN-Net on all levels of the feature pyramid. The network is trained with the Gauss-Newton loss formulation described in Section III.

**ORB-SLAM:** As an indirect method, Stereo ORB-SLAM [31] is used with default parameters. For relocalization tracking, we use the standard feature-based 2-frame pose optimization also used for frame-to-keyframe tracking. We have also tried the RANSAC scheme implemented in ORB-SLAM for relocalization, however, it yielded worse results overall. Thus we will report only the default results.

We also evaluated the Deeper Inverse Compositional Algorithm [28] on the *relocalization tracking* benchmark. However, the original implementation didn't converge despite multiple training trials with different hyperparameters.

For all our quantitative experiments we plot a cumulative distribution of the relocalization error, which is the norm of the translation between the estimated and the correct solution in meters. For each relocalization error between 0 and 1 meter, it plots the number of relocalization candidates that have been tracked with at least this accuracy.

### A. Quantitative multi-weather evaluation

We demonstrate the relocalization tracking accuracy on our new benchmark across different weathers. For these experiments, tracking is performed only across sequences with a different weather condition.

**CARLA:** For this experiment, we train on the training sequences provided by our benchmark. For all learning-based approaches, the best epoch is selected using the relocalization tracking performance on the validation set. The results on the test data are shown in Figure 5. While DSO and ORB-SLAM fail to track most of the images in the sequence, our method still performs well. Also, the large impact of our novel GN-Loss is apparent. It significantly outperforms the model trained only with the contrastive loss.

**Oxford RobotCar:** We train on the sunny and overcast condition correspondences provided by our *relocalization tracking* benchmark for the Oxford dataset. For the learning-based methods, we select the best epoch based on the relocalization tracking performance on the training set. We use the same hyperparameters that were found using the CARLA validation set. We show the results on the test data in Figure 6a. In all experiments, we observe similar results as in the CARLA benchmark. Our method significantly outperforms the baselines and our Gauss-Newton loss has a large impact as proven by the worse performance of the contrastive only model.

Figure 6b and Figure 6c show how well our model generalizes to unseen weather conditions. Despite being trained only on two sequences with overcast and sunny conditions the results for tracking against a rainy and a snowy sequence are almost the same.

<sup>1</sup><https://vision.in.tum.de/gn-net>.

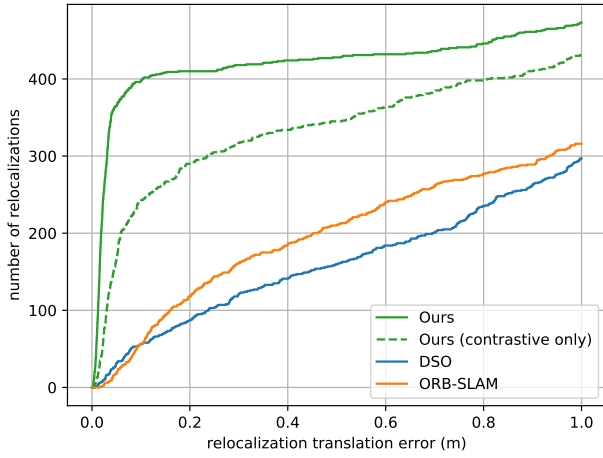


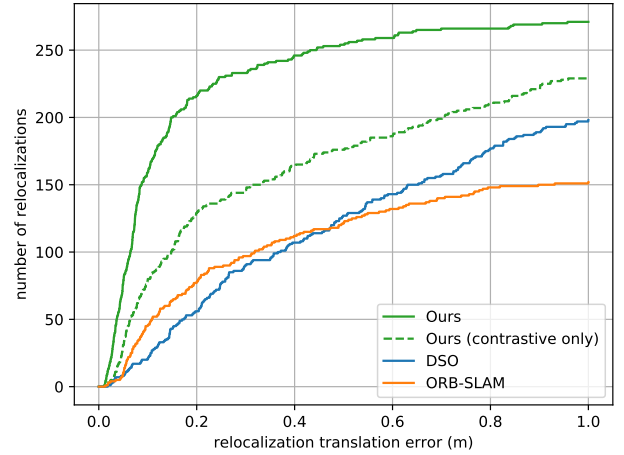
Fig. 5: This figure shows the cumulative relocalization accuracy for tracking against different weather conditions on the CARLA benchmark. ORB-SLAM is more robust to changes in lighting, and weather, whereas DSO shows the worst performance. By utilizing our trained deep descriptors, we are able to outperform both methods by a large margin. Notice that our novel Gauss-Newton loss has a large impact as the model trained only with the contrastive loss performs significantly worse.

### B. Qualitative multi-weather evaluation

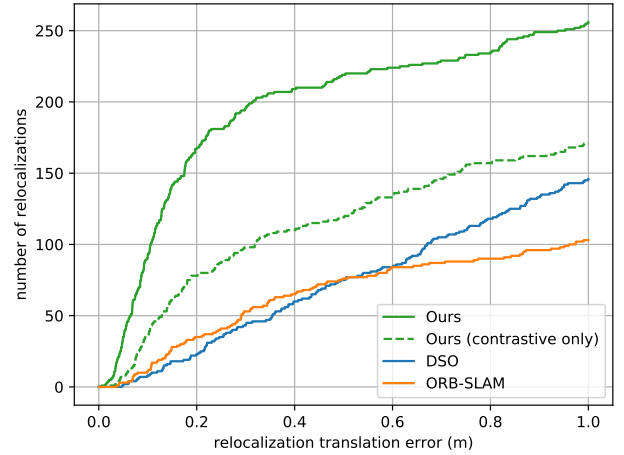
Finally, we show a relocalization demo comparing our GN-Net to DSO. For this, we load a point cloud from a sequence recorded in the sunny condition and relocalize against sequences from rainy and snowy conditions. For each keyframe, we try to track it against the nearest keyframe in the map according to the currently estimated transformation between the trajectory and the map. Figure 7 shows that the point clouds from the different sequences align nicely, despite belonging to different weather conditions. This experiment shows that our method can perform the desired operations successfully on a real-world application, including relocalization against unseen weather conditions. Figure 8, demonstrates the quantitative improvement our Gauss-Newton has over the contrastive loss actually results in a visible effect on the relocalization application. Figure 9 shows sample images used in the qualitative relocalizations.

### C. Additional experiments

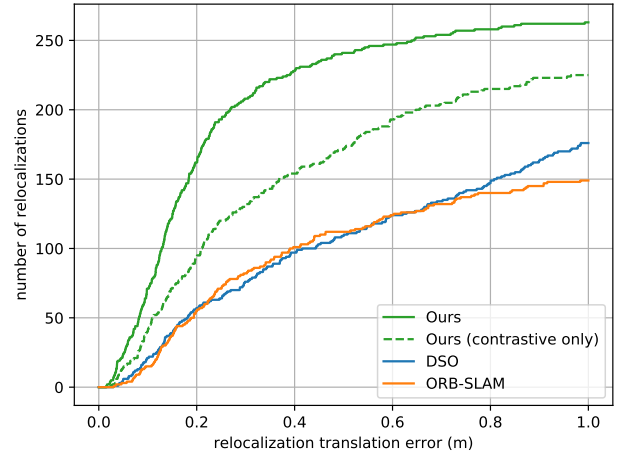
In the supplementary material, we provide more evaluations on datasets with little or no brightness variations. This includes a simpler version of our CARLA benchmark and on the EuRoC [10] dataset. We show that even in these situations our deep features significantly outperform DSO and ORB-SLAM because of their robustness to large-baselines. Especially on the EuRoC dataset, we improve the DSO performance by almost a factor of 2 for low-framerates. The supplementary material can be found at <https://vision.in.tum.de/gn-net>.



(a) Relocalization between sunny and overcast.



(b) Relocalization between sunny and rainy.



(c) Relocalization between sunny and snowy.

Fig. 6: This figure shows the cumulative relocalization accuracy on the Oxford RobotCar dataset for different sequences. Our features significantly improve the performance, especially when trained with the Gauss-Newton Loss. It is interesting to observe that despite being trained only on two sequences in overcast and sunny condition, our model still generalizes very well to even *unseen* rainy and snowy conditions.

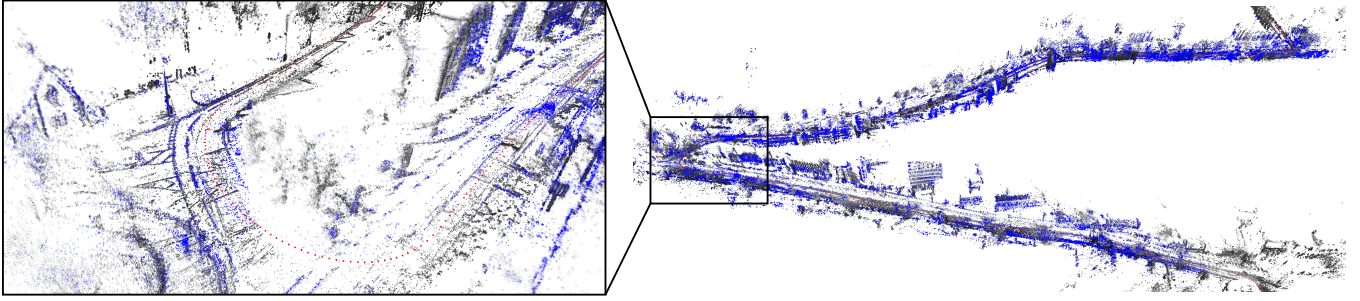


Fig. 7: This figure shows a point cloud result of our GN-Net. We relocalize a rainy sequence (blue) against a reference map created from the sunny sequence (gray).

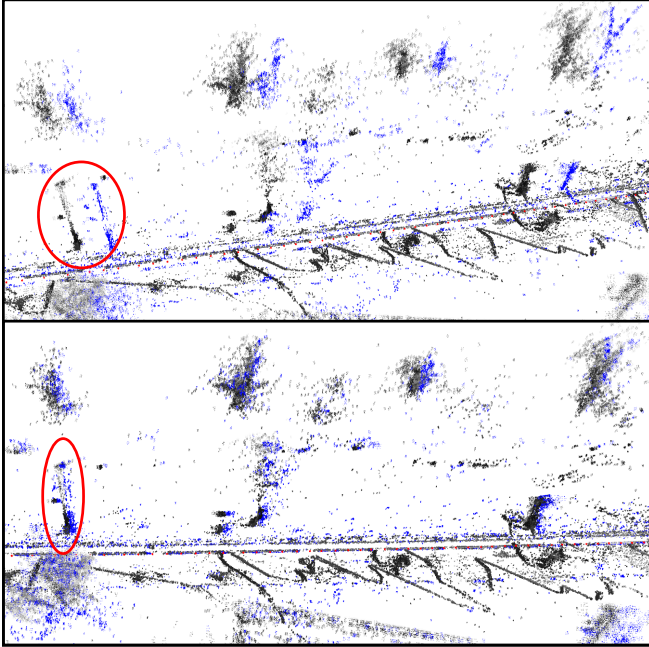


Fig. 8: Top: relocalization using the model trained with only the contrastive loss. Bottom: relocalization using the model trained with our loss formulation. This visually demonstrates the influence of the Gauss-Newton loss.

## VI. CONCLUSION & FUTURE WORK

For decades SLAM algorithms have been adjusted to work on imperfect input data, namely images. With the advent of deep learning, we can tailor the input data to be optimal for SLAM systems. This was realized by leveraging high-dimensional features trained with the Gauss-Newton loss. We find that this approach overcomes the 2 traditional disadvantages of direct methods. This makes them suitable for cases like map merging and relocalization which previously had been dominated by indirect methods.

In the future, we would like to extend this work to a complete mapping solution which allows to create and update large scale maps covering whole cities.

## REFERENCES

- [1] G. Klein and D. W. Murray, “Parallel tracking and mapping for small ar workspaces,” *2007 6th IEEE and ACM International Symposium on*



Fig. 9: This figure shows some image pairs used in the qualitative relocalizations. Left: rainy (top 2) and snowy (bottom 2) images relocalized against the sunny reference images (right).

- Mixed and Augmented Reality*, pp. 225–234, 2007.
- [2] R. Mur-Artal, J. M. Montiel, and J. D. Tardos, “ORB-SLAM: A Versatile and Accurate Monocular SLAM System,” *IEEE Transactions on Robotics*, vol. 31, no. 5, pp. 1147–1163, 2015.
- [3] J. Engel, T. Schöps, and D. Cremers, “LSD-SLAM: Large-scale direct monocular SLAM,” in *European Conference on Computer Vision (ECCV)*, 2014.
- [4] J. Engel, V. Koltun, and D. Cremers, “Direct Sparse Odometry,” *IEEE Transactions on Pattern Analysis and Machine Intelligence (TPAMI)*, vol. 40, no. 3, pp. 611–625, 2018.
- [5] H. Alismail, B. Browning, and S. Lucey, “Photometric Bundle Adjustment for Vision-Based SLAM,” in *Asian Conference on Computer Vision (ACCV)*, 2017.
- [6] M.-Y. Liu, T. Breuel, and J. Kautz, “Unsupervised Image-to-Image Translation Networks,” in *Neural Information Processing Systems*

- (NIPS), 2017.
- [7] P. Isola, J.-Y. Zhu, T. Zhou, and A. A. Efros, “Image-to-Image Translation with Conditional Adversarial Networks,” in *IEEE Conference on Computer Vision and Pattern Recognition (CVPR)*, 2017.
  - [8] H. Porav, W. Maddern, and P. Newman, “Adversarial Training for Adverse Conditions: Robust Metric Localisation using Appearance Transfer,” in *IEEE International Conference on Robotics and Automation (ICRA)*, 2018.
  - [9] T. Sattler, W. Maddern, C. Toft, A. Torii, L. Hammarstrand, E. Stenborg, D. Safari, M. Okutomi, M. Pollefeys, J. Sivic, F. Kahl, and T. Pajdla, “Benchmarking 6DOF Outdoor Visual Localization in Changing Conditions,” in *IEEE Conference on Computer Vision and Pattern Recognition (CVPR)*, 2018.
  - [10] M. Burri, J. Nikolic, P. Gohl, T. Schneider, J. Rehder, S. Omari, M. W. Achtelik, and R. Siegwart, “The EuRoC Micro Aerial Vehicle Datasets,” *The International Journal of Robotics Research (IJRR)*, vol. 35, no. 10, pp. 1157–1163, 2016.
  - [11] J. Engel, V. Usenko, and D. Cremers, “A photometrically calibrated benchmark for monocular visual odometry,” in *arXiv:1607.02555*, July 2016.
  - [12] A. Dosovitskiy, G. Ros, F. Codevilla, A. Lopez, and V. Koltun, “CARLA: An Open Urban Driving Simulator,” in *Conference on Robot Learning (CoRL)*, 2017.
  - [13] W. Maddern, G. Pascoe, C. Linegar, and P. Newman, “1 Year , 1000km : The Oxford RobotCar Dataset,” *The International Journal of Robotics Research (IJRR)*, vol. 36, no. 1, pp. 3–15, 2017.
  - [14] A. Davison, I. Reid, N. Molton, and O. Stasse, “MonoSLAM: Real-Time Single Camera SLAM,” *IEEE Transactions on Pattern Analysis and Machine Intelligence (TPAMI)*, pp. 1052–1067, 2007.
  - [15] C. Kerl, J. Sturm, and D. Cremers, “Robust odometry estimation for RGB-D cameras,” in *IEEE International Conference on Robotics and Automation (ICRA)*, 2013.
  - [16] R. A. Newcombe, S. Izadi, O. Hilliges, D. Molyneaux, D. Kim, A. J. Davison, P. Kohli, J. Shotton, S. Hodges, and A. Fitzgibbon, “KinectFusion: Real-time dense surface mapping and tracking,” in *IEEE International Symposium on Mixed and Augmented Reality (ISMAR)*, 2011.
  - [17] R. Newcombe, S. Lovegrove, and A. Davison, “DTAM: Dense tracking and mapping in real-time,” in *IEEE International Conference on Computer Vision (ICCV)*, 2011.
  - [18] S. Park, T. Schöps, and M. Pollefeys, “Illumination Change Robustness in Direct Visual SLAM,” in *IEEE International Conference on Robotics and Automation (ICRA)*, 2017.
  - [19] H. Alismail, M. Kaess, B. Browning, and S. Lucey, “Direct Visual Odometry in Low Light Using Binary Descriptors,” *IEEE Robotics and Automation Letters (RA-L)*, vol. 2, no. 2, pp. 444–451, 2017.
  - [20] C. B. Choy, J. Gwak, S. Savarese, and M. Chandraker, “Universal Correspondence Network,” in *Neural Information Processing Systems (NIPS)*, 2016.
  - [21] T. Schmidt, R. Newcombe, and D. Fox, “Self-supervised Visual Descriptor Learning for Dense Correspondence,” *IEEE Robotics and Automation Letters (RA-L)*, vol. 2, no. 2, pp. 420–427, 2017.
  - [22] P. Wohlhart and V. Lepetit, “Learning descriptors for object recognition and 3d pose estimation,” *2015 IEEE Conference on Computer Vision and Pattern Recognition (CVPR)*, pp. 3109–3118, 2015.
  - [23] C.-H. Chang, C.-N. Chou, and E. Y. Chang, “CLKN: Cascaded Lucas-Kanade Networks for Image Alignment,” in *IEEE Conference on Computer Vision and Pattern Recognition (CVPR)*, 2017.
  - [24] R. Gomez-Ojeda, Z. Zhang, J. Gonzalez-Jimenez, and D. Scaramuzza, “Learning-based image enhancement for visual odometry in challenging hdr environments,” *2018 IEEE International Conference on Robotics and Automation (ICRA)*, pp. 805–811, 2018.
  - [25] J. Czarnowski, S. Leutenegger, and A. J. Davison, “Semantic Texture for Robust Dense Tracking,” in *International Conference on Computer Vision Workshops (ICCVW)*, 2017.
  - [26] C. Tang and P. Tan, “BA-Net: Dense Bundle Adjustment Network,” *arXiv preprint arXiv:1806.04807*, 2018.
  - [27] L. Han, M. Ji, L. Fang, and M. Nießner, “Regnet: Learning the optimization of direct image-to-image pose registration,” 2018.
  - [28] Z. Lv, F. Dellaert, J. Rehg, and A. Geiger, “Taking a deeper look at the inverse compositional algorithm,” in *IEEE Conference on Computer Vision and Pattern Recognition (CVPR)*, 2019.
  - [29] M. Cummins and P. Newman, “FAB-MAP : Probabilistic Localization and Mapping in the Space of Appearance,” *The International Journal of Robotics Research (IJRR)*, vol. 27, no. 6, pp. 647–665, 2008.
  - [30] I. Kapsouras and N. Nikolaidis, “A vector of locally aggregated descriptors framework for action recognition on motion capture data,” *2018 26th European Signal Processing Conference (EUSIPCO)*, pp. 1785–1789, 2018.
  - [31] R. Mur-Artal and J. D. Tardas, “Orb-slam2: An open-source slam system for monocular, stereo, and rgb-d cameras,” *IEEE Transactions on Robotics*, vol. 33, no. 5, pp. 1255–1262, Oct 2017.
  - [32] N. Snavely, S. M. Seitz, and R. Szeliski, “Photo tourism: Exploring photo collections in 3d,” in *SIGGRAPH Conference Proceedings*. New York, NY, USA: ACM Press, 2006, pp. 835–846.
  - [33] O. Ronneberger, P. Fischer, and T. Brox, “U-Net: Convolutional Networks for Biomedical Image Segmentation,” in *Medical Image Computing and Computer-Assisted Intervention (MICCAI)*, 2015.
  - [34] B. D. Lucas and T. Kanade, “An iterative image registration technique with an application to stereo vision,” in *International Joint Conferences on Artificial Intelligence (IJCAI)*, 1981.
  - [35] A. Kendall, M. Grimes, and R. Cipolla, “PoseNet: A Convolutional Network for Real-Time 6-DOF Camera Relocalization,” in *IEEE International Conference on Computer Vision (ICCV)*, 2015, pp. 2938–2946.
  - [36] Q.-Y. Zhou, J. Park, and V. Koltun, “Open3D: A modern library for 3D data processing,” *arXiv:1801.09847*, 2018.
  - [37] R. Wang, M. Schwörer, and D. Cremers, “Stereo dso: Large-scale direct sparse visual odometry with stereo cameras,” in *International Conference on Computer Vision (ICCV)*, Venice, Italy, October 2017.